applied sciences

MDPI

Article

Dependence of Thermal Conductivity on Size and Specific Surface Area for Different Based $CoFe_2O_4$ Cluster Nanofluids

Javier P. Vallejo [1,*], Amir Elsaidy [2] and Luis Lugo [3,*]

[1] Centro Universitario de la Defensa en la Escuela Naval Militar, Grupo InTeam, Plaza de España, s/n, 36920 Marín, Spain
[2] Department of Chemical Engineering, Military Technical College, Cairo 4393010, Egypt; amiralsaidy0@gmail.com
[3] Departamento de Física Aplicada, Universidade de Vigo, 36310 Vigo, Spain
* Correspondence: jvallejo@cud.uvigo.es (J.P.V.); luis.lugo@uvigo.gal (L.L.)

Abstract: Enhancing the thermal conductivity of fluids by using nanoparticles with outstanding thermophysical properties has acquired significant attention for heat-transfer applications. Nanofluids have the potential to optimize energy systems by improving heat-transfer efficiency. In this study, cobalt ferrite nanoparticles clusters with controlled mean sizes ranging from 97 to 192 nm were synthesized using a solvothermal method to develop novel nanofluids with enhanced thermal conductivity. These clusters were comprehensively characterized using transmission electron microscopy, X-ray diffraction, Raman spectroscopy, vibrating-sample magnetometry, and nitrogen physisorption. The $CoFe_2O_4$ cluster nanofluids were prepared using the two-step method with various base fluids (water, propylene glycol, and a mixture of both). Dynamic light scattering analyses of the average Z-size of the dispersed nanoadditives over time revealed that the stability of the dispersions is influenced by cluster size and the proportion of glycol in the base fluid. The thermal conductivity of the base fluid and nine different 0.5 wt% $CoFe_2O_4$ cluster nanofluids was measured using the transient hot wire method at temperatures of 293.15, 303.15, and 313.15 K, showing different temperature dependencies. The study also explores the relationships between the thermal conductivity, cluster size, and specific surface area of the nanoadditives. A maximum thermal conductivity enhancement of 4.2% was reported for the 0.5 wt% nanofluid based on propylene glycol containing 97 nm $CoFe_2O_4$ clusters. The findings suggest that the specific surface area of nanostructures is a more relevant parameter than size for describing improvements in thermal conductivity.

Keywords: clusters; $CoFe_2O_4$; solvothermal; SSA; thermal conductivity

check for updates

Citation: Vallejo, J.P.; Elsaidy, A.; Lugo, L. Dependence of Thermal Conductivity on Size and Specific Surface Area for Different Based $CoFe_2O_4$ Cluster Nanofluids. *Appl. Sci.* **2024**, *14*, 9954. https://doi.org/10.3390/app14219954

Academic Editors: Guice Yao, Chuang Wen and Jin Zhao

Received: 27 September 2024
Revised: 25 October 2024
Accepted: 28 October 2024
Published: 31 October 2024

Copyright: © 2024 by the authors. Licensee MDPI, Basel, Switzerland. This article is an open access article distributed under the terms and conditions of the Creative Commons Attribution (CC BY) license (https://creativecommons.org/licenses/by/4.0/).

1. Introduction

Poor thermal conductivity of base fluids (commonly mineral oils, water and/or glycols) establishes a barrier to the creation of advanced energy-efficient heat-transfer equipment. Therefore, improving the efficiency of heat transfer of these conventional fluids is nowadays a critical issue at the industrial level. Generally, nanofluids are considered as a novel kind of heat-transfer fluid with nanosized additives dispersing into conventional working fluids [1]. The impact of using heat-transfer fluids with dispersed nanoparticles with important effects on intrinsic parameters and thermal performance behaviours [2–4] has opened the door for the improvement of energy-efficient heat-transfer devices [5–8].

The presence of nanomaterials in the fluid implies changes in thermal conductivity, which is the most crucial factor influencing heat transfer and plays a significant role in the advancement of heat-transfer systems [8]. Other key parameters such as thermal diffusion, density, and surface tension are also directly involved in numerous industrial applications associated with solar- and thermal-energy supply, heat pipes, or cooling fluids [9–16]. Nanoparticles are nanosized materials with unique characteristics that make them attractive, particularly their outstanding thermophysical properties when compared with bulk

materials [5,6]. Due to the nano sizes and very large specific surface areas of these particles, nanofluids overcome problems related to systems of microparticles and base fluids [7]. Nanoparticles of diverse materials have been used for the production of nanofluids [17,18], with the promise of a rather large surface/volume ratio and a large number of nanoparticles interacting with the surrounding fluid to promote heat flow. Furthermore, the nanometric size minimizes the gravitational effects, thus avoiding problems related to sedimentation. Therefore, metals—Cu, and Fe [17], metal oxides—Al_2O_3, CuO, SiO_2, TiO_2, and ZrO_2, carbon materials—carbon nanotubes and graphene—or hybrid nanoparticles [18], among others, were used in the design of nanofluids.

On the other hand, the aggregation of nanoparticles has become a challenge in the field of nanofluids. Aggregation refers to the clumping or sticking together of the dispersed colloid particles to form aggregates or flocks [19]. These structures, made up of primary particles, can remain loosely tied together, and have been demonstrated to have both beneficial and detrimental effects in the final thermophysical properties of nanofluids [20,21]. In addition, the stability of nanoparticle aggregation in the dispersion is crucial and significant analyses must be undertaken in this area [22,23]. However, since there is a lack of control over the possible aggregation of nanoparticles above a maximum concentration when dispersed in base fluids intended for use in heat exchangers, the impact of controlled aggregation on the thermal characteristics of nanofluids has not yet been sufficiently investigated.

To shed some light on this, we have recently opened a line of research focused on the effect of a controlled aggregation of nanosized iron oxide on the properties of nanofluids [24]. Nevertheless, finding an effective way to exert control over an aggregation process is not an easy task, considering the two steps necessary: firstly, bringing together the nanoparticles and secondly, keeping a similar number of them sticked when they do make contact to form clusters. Furthermore, when clusters are formed, the ideal case is that they grow solely by adding more individual nanoparticles, but cluster–cluster aggregation can also occur [19]. There have been significant advances in this regard in colloidal synthesis, which have enabled the use of nanoparticles as "artificial atoms" to build novel materials that integrate the size- and shape-dependent characteristics of individual nanoparticles while also generating unique combined properties via their interactions when organized into clusters [25]. The solvothermal synthesis of clusters stands out, due to the relatively simple steps and setups required and the low energy requirements, and despite the limited scalability and absence of options for direct observation of the reaction process. Clusters of transition metal oxides such as Fe_3O_4/γ-Fe_2O_3, $MnFe_2O_4$, $CoFe_2O_4$ and $ZnFe_2O_4$ have been successfully produced using this method, which allows for an effective tuning of the size of both clusters and the nanoparticles that compose them [26,27], taking into account a two-stage growth process: initially, the nucleation of nanocrystals and, subsequently, the consistent and controlled aggregation into larger nanostructures [20].

These aggregates or clusters of nanoparticles can offer alternative ways to increase thermal efficiency, given the different arrangement of the nanoparticles that create a particular solid–liquid interface through which heat transfer is promoted, whose extension is also tuned in the final nanofluid when considering different average size or concentration of clusters. This research reports on the synthesis of clusters of cobalt ferrite nanoparticles with customized average sizes (from 97 to 192 nm) via the solvothermal method. The formation of the spinel cobalt ferrite magnetic phase was confirmed by X-ray diffraction (XRD), Raman spectroscopy (RS) and vibrating-sample magnetometry (VSM). The effective adjustment of the average size of the clusters was checked by transmission electron microscopy (TEM), while the specific surface area (SSA) of the clusters was examined by nitrogen physisorption. Moreover, these clusters were dispersed in different base fluids, with the purpose of studying the influence of this particular solid–liquid interface created between the magnetic material arranged in clusters and the fluid under consideration in the thermal conductivity of novel nanofluids.

2. Materials and Methods

2.1. Chemicals

Iron(III) chloride hexahydrate ($FeCl_3 \cdot 6H_2O$), cobalt chloride hexahydrate ($CoCl_2 \cdot 6H_2O$), sodium acetate poly(ethylene glycol) (PEG 6000), ethylene glycol (EG), and propylene glycol (PG) with >99% purity were acquired from Sigma-Aldrich (Darmstadt, Germany), and water (Milli-Q, Molsheim, France) was produced in the lab. All chemicals were utilized without changes.

2.2. Synthesis of Nanoparticles

The synthesis of clusters of cobalt ferrite ($CoFe_2O_4$) nanoparticles with tuneable final sizes was achieved by a modified synthetic process previously reported [28]. For the three samples of clusters under consideration, 2.5 mmol $CoCl_2$ $6H_2O$ and 5 mmol $FeCl_3 \cdot 6H_2O$ were dissolved in 20 mL of EG followed by the addition of 3.6 g of sodium acetate (CH_3COONa) and PEG 6000, in three independent experiments with magnetic stirring. Then, the mixture was stirred for 30 min at 323 K to obtain a homogeneous solution. To adjust the ultimate size of the clusters, the amounts of PEG 6000 used were 3, 2 and 1.25 wt%. The average sizes of the designed clusters were then determined, correspondingly. Thus, cluster A (97 nm), cluster B (155 nm) and cluster C (192 nm) were obtained, respectively. In all cases, the mixture was enclosed in a stainless-steel autoclave and heated to 453 K with a heating rate of 5 K/min, while the solution was mechanically stirred at 500 rpm for 16 h. Subsequently, the mixture was allowed to cool to ambient temperature, and the black precipitate was retrieved via a magnet. All clusters were subsequently rinsed with Milli-Q water and dried in an oven for around 12 h at 333 K for further characterization.

2.3. Preparation of Nanofluids

The design of the nanofluids was developed through a two-step process. The base fluids were Milli-Q water (W), propylene glycol (PG) and a mixture of PG and W at a mass ratio of 35:65 (PG:W). Nanofluids were prepared at 0.1 and 0.5 wt% concentrations of the three synthetized nanoadditives (cluster A, cluster B and cluster C). The nomenclature used to name the designed nanofluids from now on is summarized in Table 1. The corresponding amounts of base fluid and nanoadditives were suitably weighed using an analytical balance. Following the mixing process, the samples were subjected to sonication by an Ultrasons ultrasonic bath from JP Selecta (Barcelona, Spain) for 15 min at 200 W and 20 kHz.

Table 1. List of designed nanofluids.

Cluster	Base Fluid	Nanofluid Name
A (97 nm)	Water	$CoFe_2O_4$ 97 nm/W
A (97 nm)	Propylene glycol	$CoFe_2O_4$ 97 nm/PG
A (97 nm)	Propylene glycol:water at 35:65 mass ratio	$CoFe_2O_4$ 97 nm/PG:W
B (155 nm)	Water	$CoFe_2O_4$ 155 nm/W
B (155 nm)	Propylene glycol	$CoFe_2O_4$ 155 nm/PG
B (155 nm)	Propylene glycol:water at 35:65 mass ratio	$CoFe_2O_4$ 155 nm/PG:W
C (192 nm)	Water	$CoFe_2O_4$ 192 nm/W
C (192 nm)	Propylene glycol	$CoFe_2O_4$ 192 nm/PG
C (192 nm)	Propylene glycol:water at 35:65 mass ratio	$CoFe_2O_4$ 192 nm/PG:W

2.4. Characterizations

Transmission electron microscopy (TEM) study was conducted using a JEOL JEM 1010 apparatus (Tokyo, Japan) working at 100 kV acceleration voltage. The studied samples were obtained by depositing a diluted solution of the nanoparticles on a thin carbon-coated copper grid. The patterns of the X-ray diffraction (XRD) analysis were obtained by a Siemens D-5000 powder X-ray diffractometer (Karlsruhe, Germany) with CuKα radiation (wavelength of 1.54056 Å) throughout the 2θ range of 5° to 100° and compared with the

crystallographic information files of the crystallographic open database. The gathered data were refined with the Le Bail technique via the Rietica program. Raman spectra were obtained from powdered materials on a glass slide substrate, using a Renishaw in Via Reflex Raman Microscope (Gloucestershire, UK). Experiments were performed at ambient temperature with an excitation wavelength of 633 nm. Magnetic tests were conducted by a Quantum Design MPMS XL7 SQUID physical property measurement system (San Diego, CA, USA) supported with a vibrating-sample magnetometer. Field-dependent magnetization curves were recorded at 300 K, with an external field of up to 7 T. The specific surface area (SSA) of the clusters was characterized by a Micromeritics ASAP 2020 analyzer (Norcross, GA, USA) using nitrogen physisorption at 77 K and applying the Brunauer–Emmett–Teller (BET) theory. Before each analysis, the materials were degassed for 240 min at 513 K in vacuum.

The stability of the nanofluids was assessed via dynamic light scattering using a Malvern Instruments ZetasizerNano ZS (Malvern, UK). The average Z-size (i.e., the intensity-weighted average hydrodynamic size obtained from a cumulant fit of the intensity autocorrelation function) of the samples was determined over 16 days at 173° scattering angle and 298.15 K. The analysis was carried out for the 0.1 wt% $CoFe_2O_4$ 97 nm/W, $CoFe_2O_4$ 97 nm/PG:W, $CoFe_2O_4$ 192 nm/W, and $CoFe_2O_4$ 192 nm/PG:W nanofluids with a double objective, which was to observe the behaviour (1) with an increasing amount of PG in the base fluid and (2) with the increasing size of the clusters. Two samples with different conditions were analysed for each cited nanofluid. One remained in static state after preparation (hereinafter, static nanofluid) and the other was mechanically stirred for 60 s at 2000 rpm before measurement (hereinafter, shaken nanofluid) using a VELP ZX3 vortex mixer (Usmate Velate, Italy).

The thermal conductivities of the base fluids and nanofluids at 293.15, 303.15 and 313.15 K were obtained using a Thermtest THW-L2 device (Hanwell, NB, Canada) with a Peltier EchoTherm IC20XR dry bath (Hartkirchen, Austria), which ensured a constant temperature. The experimental method of the thermal conductivity meter employs the transient hot wire approach, as per ASTM D7896-19 [29]. The principal element of the device is a 60 mm long and 0.1 mm diameter alumel wire, which is submerged in a container containing roughly 20 mL of sample. The wire is heated using a constant current source, and the temperature increase is measured by observing the change in the wire's electrical resistance. Short input times (10 s) and low heat powers (70–200 mW) were used to obtain low temperature rises (~2.3 °C) within the tested fluid, in order to avoid natural convection. More details about the device and measurement technique can be found in Refs. [24,30,31]. The obtained thermal conductivity values have a 2% extended uncertainty.

3. Results and Discussion

3.1. Morphology and Structure of the Clusters

The clusters of cobalt ferrite ($CoFe_2O_4$) nanoparticles herein studied were acquired by means of a solvothermal method, which, by tuning the PEG 6000 amount in the reaction medium [24,32], allows for the production of clusters with different average size. Figure 1 includes overview images from the transmission electron microscopy (TEM) of the samples of clusters employed, as well as the three different forms of cluster analysed in terms of their size distribution (Gaussian fit): A, B and C, with average diameters of 97 ± 23 nm, 155 ± 34 nm and 192 ± 38 nm, respectively.

Figure 2 comprises the structural and magnetic characterization of the designed clusters, taking in consideration X-ray diffraction (XRD), Raman spectroscopy and vibrating sample magnetometry (VSM). The XRD analysis of the clusters from the different samples shows three similar patterns (Figure 2a), where we find distinct peaks that may be associated with a spinel structure. The observed peaks correspond to (220), (311), (400), (511) and (440) diffracted planes of this cubic structure, taking into account the $CoFe_2O_4$ bulk of the normal spinel structure. The lattice parameter derived from the refining of these data via the Le Bail technique is a = 0.8380 nm (with very small variations between the three samples),

which is compatible with that previously reported for cobalt ferrite nanoparticles [33]. The different intensity ratios between diffracted peaks, comparing the three samples, can be explained in terms of the average size of the nanoparticles of $CoFe_2O_4$ forming the final clusters [20].

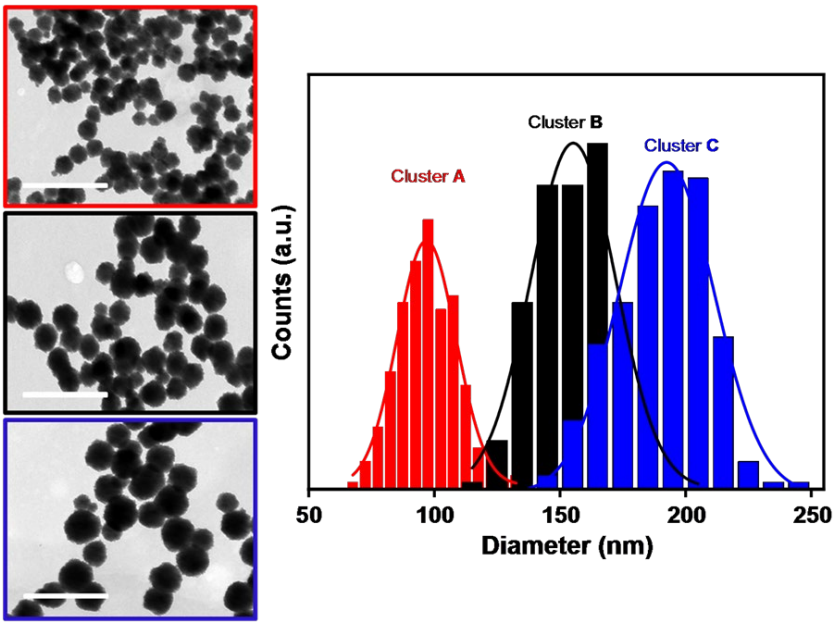

Figure 1. TEM images at 12,000× magnification (scale bar, 500 nm) and particle size distribution of clusters A (red), B (black) and C (blue).

A complementary analysis of the crystalline structure of the samples was performed using Raman spectroscopy, since it can provide paired information, for example, in terms of different cationic arrangements in the spinel crystalline structure [34,35]. Given the nature of the samples, an excitation wavelength of 633 nm was employed. Figure 2b includes the Raman spectra of the three nanostructures, indicating the typical group-theory vibration modes of $CoFe_2O_4$ (dotted lines), the T_{2g} (1) (not included), E_g, T_{2g} (2), T_{2g} (3), A_{1g} (1) and A_{1g} (2) modes, as in Ref. [36]. The Raman bands observed for the three samples at 300 (E_g), 470 (T_{2g} (2)), 565 (T_{2g} (3)), 621 (A_{1g} (1)) and 680 (A_{1g} (2)) cm^{-1}, match these vibration modes expected, and confirm the $CoFe_2O_4$ as the main component of the three samples of clusters.

For a matching confirmation, the magnetic properties of the designed samples were checked by vibrating sample magnetometry. Figure 2c includes the field-dependent magnetization at ambient temperature of the synthesized clusters A, that is, with an average diameter of 97 ± 23 nm, and formed by very small nanoparticles. The value (76 Am^2/kg) of saturation magnetization registered when applying a magnetic field up to 7 T is very close to the value of bulk cobalt ferrite (~80 Am^2/kg) and the small difference can be argued considering the magnetic dead layer of nanoparticles, which slightly decreases the magnetic response per mass of sample. The lack of coercivity in this type of cluster stems from the superparamagnetic behaviour, given the very small size of the nanoparticles forming the clusters themselves [37].

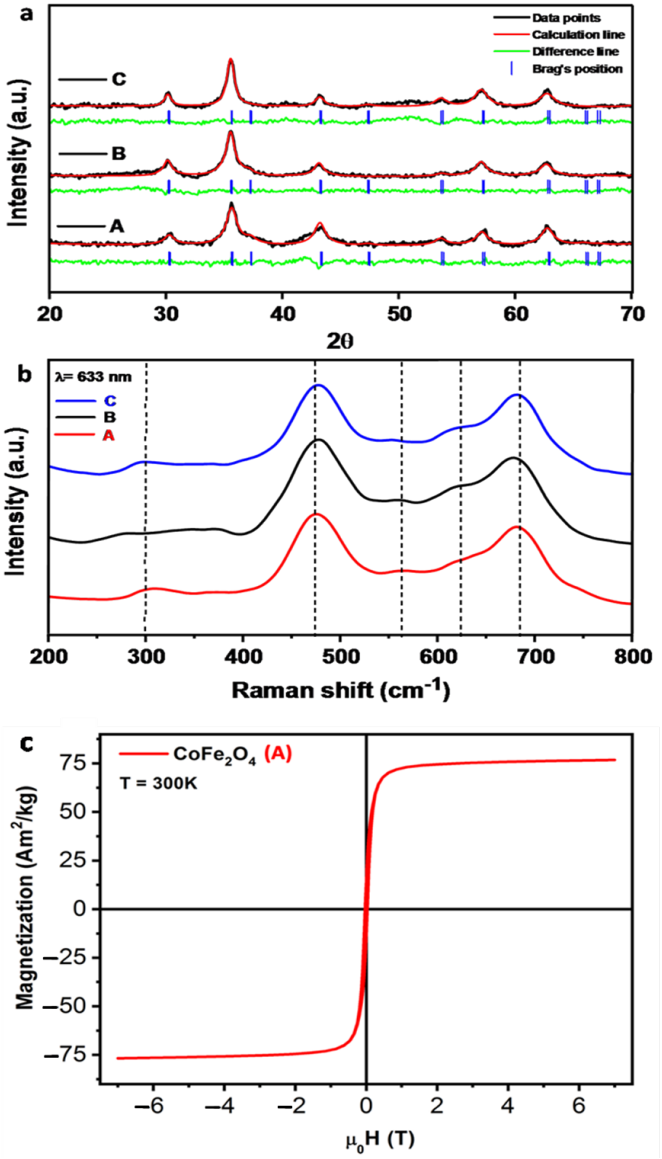

Figure 2. (**a**) XRD patterns of clusters A, B and C, (**b**) Raman spectra obtained with a 633 nm excitation wavelength, and (**c**) field-dependent magnetization of cluster A, registered at 300 K.

3.2. Stability of the Nanofluids

The stability of nanofluids is a significant feature that may decrease their applicability in engineering processes. Its characterization has been experimentally addressed in the literature through zeta potential analyses, UV–visible spectroscopy, electron microscopy, or sedimentation techniques, among others [38]. Our group has previously verified that light scattering measurements of average Z-size against time after preparation are an effective and consistent method for characterizing the stability of a dispersion of nanoparticles [24,39].

Figure 3 shows the time variation of the average Z-size for various 0.10 wt% W- and PG:W-based nanofluids. Figure 3a evidences quasi-constant values for both different-sized cluster aqueous nanofluids under shaken conditions during the 16 days of analysis. Nevertheless, the static aqueous samples show a size decrease with time, which is more pronounced for the sample that contains larger-sized clusters (192 nm). Figure 3b also shows a nearly constant value for both shaken PG:W-based nanofluids. However, the static samples show a less-marked decrease with time, which is slight for the nanofluids that include smaller-sized clusters (97 nm). Therefore, the stability analysis evidences the fact

that moderately stable nanofluids with readily recovered initial-dispersion conditions were achieved. The lowest-sized clusters remain better dispersed over time and the increasing amount of propylene glycol in the base fluid seems to favour the stability of the dispersions, as can also be observed visually.

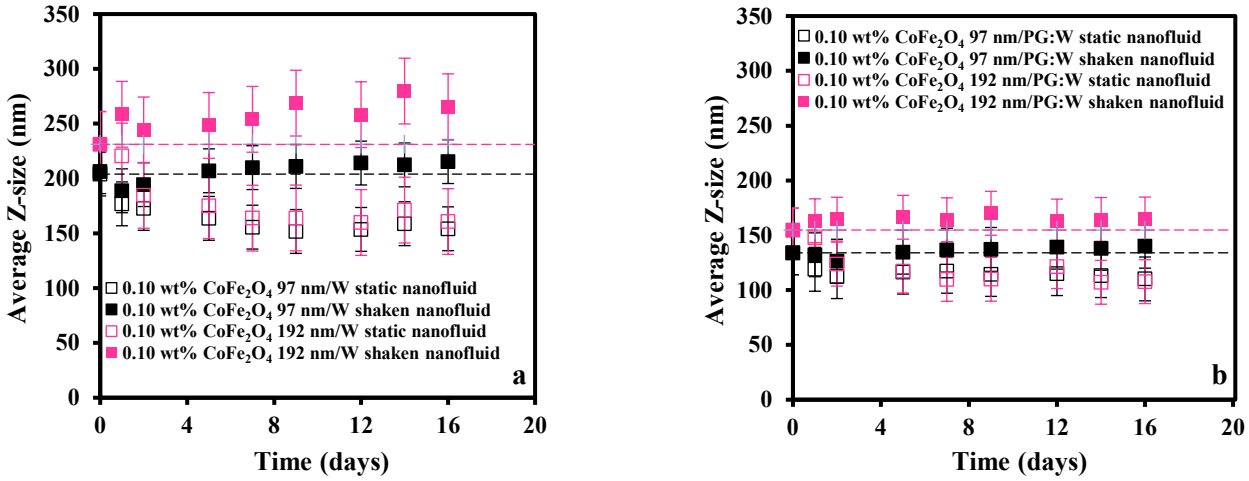

Figure 3. Average Z-size versus time from preparation for the 0.10 wt% (**a**) W-based and (**b**) PG:W-based static and shaken nanofluids.

3.3. Thermal Conductivity

The experimental values of thermal conductivity obtained for the base fluids (W, PG:W and PG) and shown in Table 2 exhibit strong concordance with the literature data. Average deviations of 0.5% (W), 0.9% (PG:W) and 1.2% (PG) were obtained with respect to Lemmon et al. [40], Melinder [41] and Sun and Teja [42], respectively.

Table 2. Experimental thermal conductivity of the base fluids and the difference-based nanofluids for various cluster sizes and temperatures.

Nanofluid Set	Temperature [K]	Thermal Conductivity [W/(m·K)]			
		Base Fluid	0.50 wt% $CoFe_2O_4$ 97 nm Nanofluid	0.50 wt% $CoFe_2O_4$ 155 nm Nanofluid	0.50 wt% $CoFe_2O_4$ 192 nm Nanofluid
W-based	293.15	0.601	0.616	0.607	0.605
	303.15	0.619	0.635	0.627	0.625
	313.15	0.636	0.653	0.645	0.641
PG:W-based	293.15	0.418	0.433	0.429	0.424
	303.15	0.426	0.443	0.437	0.432
	313.15	0.433	0.450	0.443	0.438
PG-based	293.15	0.200	0.207	0.204	0.202
	303.15	0.199	0.206	0.204	0.202
	313.15	0.197	0.205	0.202	0.200

Figure 4 and Table 2 show the obtained experimental thermal conductivities for the different nanofluid sets. A decreasing trend with the increasing size of cluster is observed, with maximum thermal conductivity increases of 2.6%, 3.9% and 4.2% for W-, PG:W- and PG-based nanofluids, respectively. It should be noted that the reported behaviour is evidenced for all the temperatures analysed.

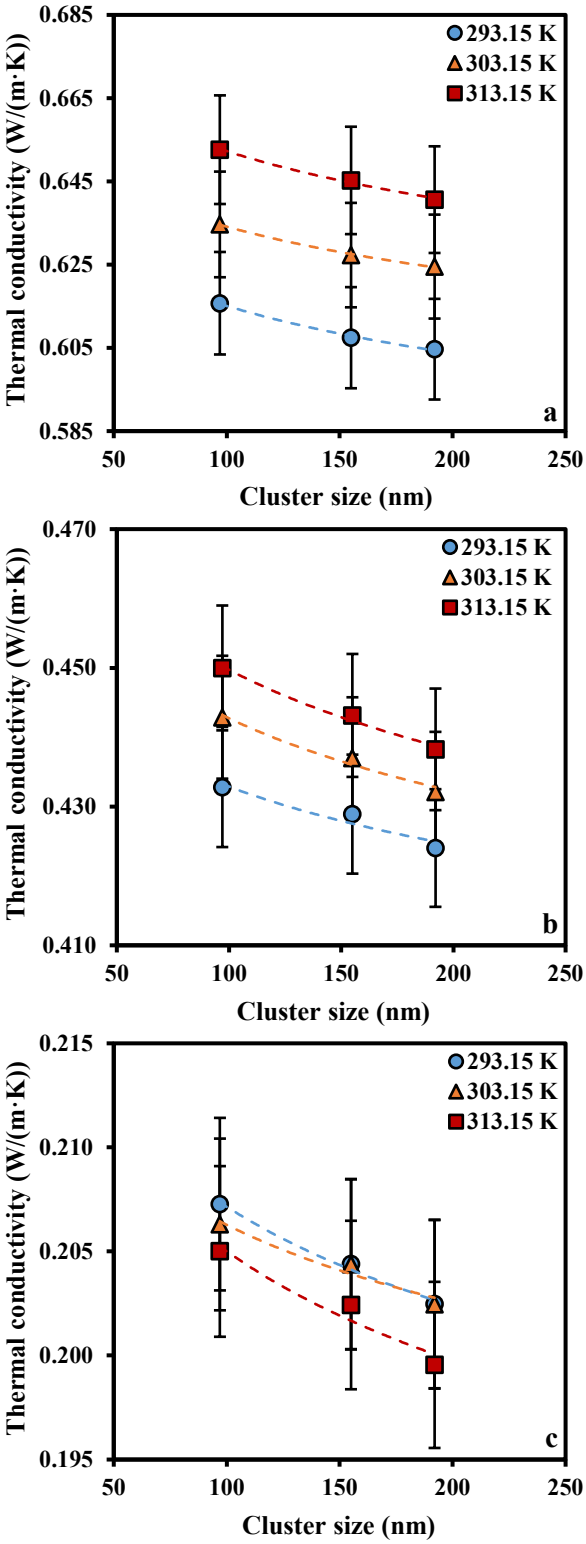

Figure 4. Thermal conductivities as a function of size of cluster for W (**a**), PG:W (**b**) and W-based (**c**) nanofluids.

Several authors reported an indirect relation between thermal conductivity of nanofluids and size of metal oxide nanoparticles: Chon et al. [43], Li and Peterson [44], Mintsa et al. [45], Lee et al. [46] or Patel et al. [47] for Al_2O_3/water nanofluids; He et al. [48] and Maheshwary et al. [49] for TiO_2/water nanofluids; Kim et al. [50] for TiO_2/ethylene glycol (EG) and ZnO/EG nanofluids; Timofeeva et al. [51] for Al_2O_3 dispersions in an EG and W

mixture at 50:50 wt%; and Vajjha and Das [52] for Al_2O_3, Cu_2O and ZnO dispersions in an EG and W mixture at 40:60 wt%.

Nevertheless, other authors reported the contrary trend, a direct relation between thermal conductivity of nanofluids and size of metal oxide nanoparticles: Chen et al. [53] and Sun et al. [54] for SiO_2/water nanofluids; Murshed et al. [55] for TiO_2/water nanofluids; Pryazhnikov et al. [56] for Al_2O_3, SiO_2, TiO_2, ZrO_2, and CuO/water nanofluids; or Satti et al. [57] for Al_2O_3, SiO_2, TiO_2, ZnO, and CuO dispersions in a PG and W mixture at 40:60 wt%. Our previous work [24] on aqueous dispersions of Fe_3O_4/γ-Fe_2O_3 clusters also showed this direct relationship.

Ambreen and Kim concluded recently, in a review [58], that most studies found that the thermal conductivity of nanofluids increases as the particle size decreases (especially below 100 nm). They also affirm that the theoretical explanations by interfacial fluid layering, particle clustering, Brownian motion and nano-convection justify this indirect relation between thermal conductivity and size.

Figure 4a,b evidence that a temperature rise leads to a thermal conductivity increase for both W- and PG:W-based nanofluids, respectively. These increases are around 6% for the former and 3–4% for the latter, which are very similar to those experienced by the corresponding base fluids. However, PG-based nanofluids show practically the same thermal conductivity values at 293.15 and 303.15 K (maximum 1% discrepancy within the temperature increase from 293.15 and 303.15 K), in accordance with the behaviour of pure PG. These findings are consistent with Beck et al. [59], who conclude how thermal conductivity varies as a function of temperature follows that of the base fluid (in their work: water, EG and EG:W mixtures).

Figure 5 shows that the nanofluid thermal conductivity improvements of the nine analysed nanofluids are practically independent of temperature. This behaviour is observed consistently across different base fluids, suggesting that the influence of temperature on microconvection effects and Brownian motion is minimal within the range studied. The stability of the nanofluid dispersions likely plays a crucial role in maintaining this temperature-independent behaviour, as a stable dispersion ensures consistent nanoparticle contribution across temperatures. This finding aligns with previous observations reported by our group [24,60,61], but it is important to note that the literature on this topic remains divided. Some studies corroborate our findings of temperature independence [62–64], while others report variations in conductivity enhancements with temperature [7,65–67], particularly at higher temperature ranges. The observed stability in our experiments might be related to the controlled conditions and optimized dispersion quality, as high concentrations or elevated temperatures could compromise dispersion stability and result in varying thermal conductivity behaviour.

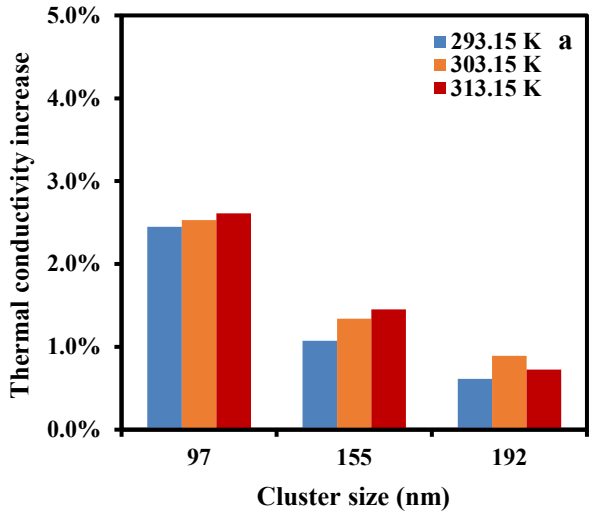

Figure 5. *Cont.*

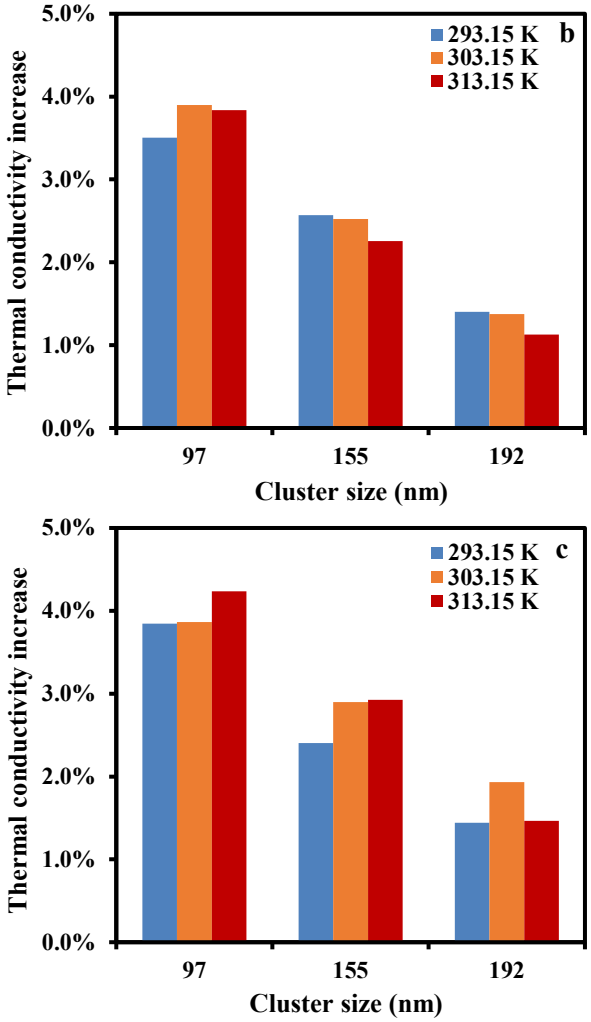

Figure 5. Thermal conductivity enhancements as a function of size of cluster for (**a**) W, (**b**) PG:W and (**c**) PG-based nanofluids.

Figure 6 shows the improvements in nanofluids' thermal conductivity as a function of their own thermal conductivities. As can be seen, PG-based nanofluids show the highest enhancements for all cluster sizes, W-based nanofluids show the lowest enhancements, and PG:W-based nanofluids show intermediate improvements. This enables us to deduce that the lower the thermal conductivity of the base fluid, the greater the enhancement for the same size and mass concentration of a nanoadditive. A similar trend was previously reported by our group for the dynamic viscosity of nanofluids [68]: as the dynamic viscosity of the base fluid decreases, the enhancement for a given mass concentration of nanoadditive increases. The results evidenced here for thermal conductivity extend this theory to more transport properties of nanofluids.

The specific surface area (SSA) of a particle is a function of size, shape, porosity, pore size distribution, and roughness. Das affirmed in a review [69] that several researchers accept that a smaller size of nanoparticle shows higher thermal-conductivity improvement, due to the high SSA observed. In order to explain the different trend here obtained for $CoFe_2O_4$ cluster aqueous nanofluids, and in our previous work [24] for Fe_3O_4/γ-Fe_2O_3 cluster aqueous nanofluids, Figure 7 shows the SSA of different-sized clusters of both types after being distributed in the base fluid (water) and then allowed to dry. In both cases, the higher thermal-conductivity increase corresponds to the clusters with higher SSA between those analysed: the smaller-sized clusters of $CoFe_2O_4$ and the larger-sized clusters of Fe_3O_4/γ-Fe_2O_3.

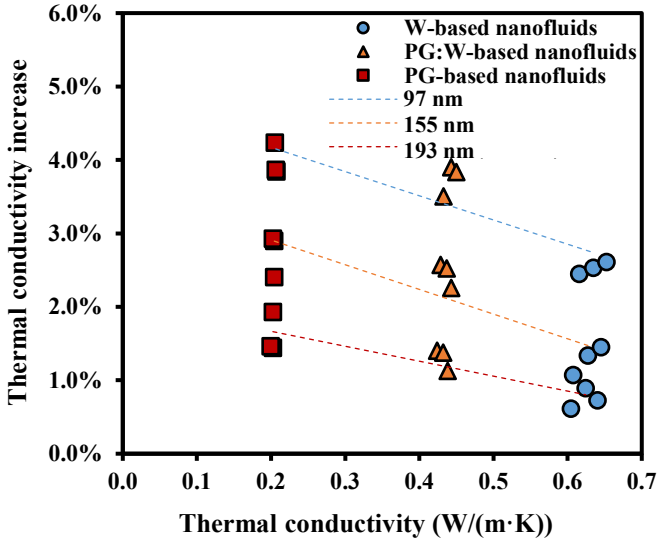

Figure 6. Thermal conductivity-enhancement dependence on the thermal conductivity range of $CoFe_2O_4$-based nanofluids.

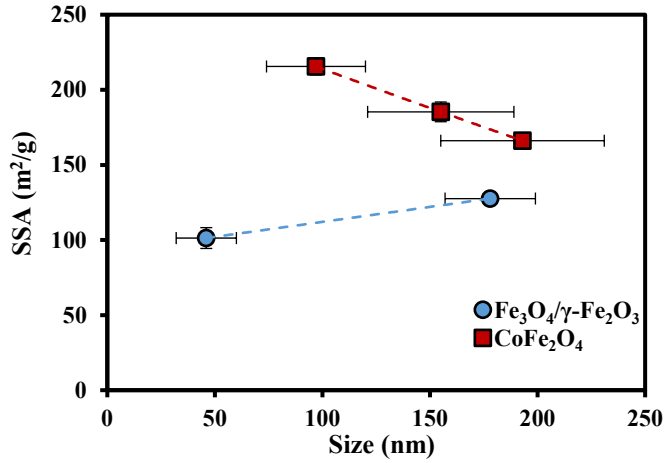

Figure 7. Specific surface area (SSA) as a function of TEM size for the clusters of Fe_3O_4/γ-Fe_2O_3 [24] and $CoFe_2O_4$ [this work].

The findings indicate a clear correlation between the thermal conductivity of the nanofluid and the SSA of the nanoadditive. However, the increasing or decreasing nanoadditive size (observed after synthesis, before being dispersed) may not imply an obvious trend in the thermal conductivity of the nanofluid. SSA should be enlarged by increasing the particle size while maintaining the rest of the parameters involved. However, the effect of changes in shape, porosity, or roughness may have a greater influence on SSA than size increase. Thus, nanoadditive SSA could become a preferred parameter before size for nanoadditive selection, but not the only one. The type of material and the stability of the dispersion, among other variables, will also have a great influence on the improvement in thermal conductivity. Likewise, the observed enhancements could be beneficial for various heat-transfer applications, such as improving the efficiency of heat exchangers, solar energy collectors, and cooling systems. These improvements are in line with the broader goal of optimising energy systems by exploiting the unique properties of nanofluids.

4. Conclusions

In this study, the following features were achieved:

- Clusters of cobalt ferrite ($CoFe_2O_4$) nanoparticles (a novelty in nanofluid design) with average diameters of 97 to 192 nm were synthesized by a solvothermal method, adjust-

ing the amount of poly(ethylene glycol) in the reaction medium. Their morphology and structure were confirmed by TEM, XRD, Raman spectroscopy (RS), and vibrating sample magnetometry (VSM).

- Nanofluids were designed with different base fluids [water (W), propylene glycol (PG) and PG:W] at 0.1 and 0.5 wt% concentrations of the three synthesized nanoadditives ($CoFe_2O_4$ 97 nm, $CoFe_2O_4$ 155 nm, and $CoFe_2O_4$ 192 nm).
- The DLS analyses of the average Z-size over time evidence moderately stable nanofluids with readily recoverable initial dispersion conditions. The smaller size of the nanoadditive and the greater amount of PG favour dispersion stability.
- The analysis of the thermal conductivity of the nanofluids reveals temperature-dependences similar to those of the corresponding base fluid. W- and PG:W-based nanofluids obtain larger values as temperature rises, while PG-based nanofluids obtain similar values within the studied temperature range.
- The nanofluid thermal-conductivity enhancements are practically temperature-independent.
- The lower the thermal conductivity of the base fluid, the greater the enhancement for the same nanoadditive and mass concentration.
- The SSA becomes a more preferable parameter than size to describe the thermal conductivity improvements. The thermal conductivity of the $CoFe_2O_4$ cluster nanofluids shows decreases as the SSA decreases (the size increases) for all base fluids. A maximum enhancement of 4.2% is reported for the 0.5 wt% $CoFe_2O_4$ 97 nm/PG nanofluid.

Author Contributions: Conceptualization, J.P.V. and L.L.; methodology, J.P.V. and L.L.; validation, J.P.V. and L.L.; formal analysis, J.P.V., A.E. and L.L.; investigation, J.P.V. and A.E.; resources, J.P.V. and L.L.; data curation, J.P.V. and A.E.; writing—original draft preparation, J.P.V. and A.E.; writing—review and editing, J.P.V. and L.L. All authors have read and agreed to the published version of the manuscript.

Funding: Grant PID2020-112846RB-C21 funded by MCIN/AEI/10.13039/501100011033. Grant PDC2021-121225-C21 funded by MCIN/AEI/10.13039/501100011033 and by "European Union NextGenerationEU/PRTR".

Institutional Review Board Statement: Not applicable.

Informed Consent Statement: Not applicable.

Data Availability Statement: The original contributions presented in the study are included in the article, further inquiries can be directed to the corresponding author.

Acknowledgments: J.P.V. thanks the Defense University Center at the Spanish Naval Academy (CUD-ENM) for all the support provided for this research.

Conflicts of Interest: The authors declare no conflicts of interest.

References

1. Sun, L.; Geng, J.; Dong, K.; Sun, Q. An Experimental Study on the Effect of Nanofluids on the Thermal Conductivity and Rheological Properties of a Coolant for Liquids. *Energies* **2024**, *17*, 1313. [CrossRef]
2. Xie, H.; Fujii, M.; Zhang, X. Effect of interfacial nanolayer on the effective thermal conductivity of nanoparticle-fluid mixture. *Int. J. Heat Mass Transf.* **2005**, *48*, 2926–2932. [CrossRef]
3. Eastman, J.A.; Choi, S.U.S.; Li, S.; Thompson, L.J.; Lee, S. Enhanced thermal conductivity through the development of nanofluids. *MRS Online Proc. Libr. (OPL)* **1996**, *457*, 3. [CrossRef]
4. Choi, S.U.S.; Zhang, Z.G.; Yu, W.; Lockwood, F.E.; Grulke, E.A. Anomalous thermal conductivity enhancement in nanotube suspensions. *Appl. Phys. Lett.* **2001**, *79*, 2252–2254. [CrossRef]
5. Murmu, P.P.; Shettigar, A.; Chong, S.V.; Liu, Z.; Goodacre, D.; Jovic, V.; Takao, M.; Smith, K.E.; Kennedy, J. Role of phase separation in nanocomposite indium-tin-oxide films for transparent thermoelectric applications. *J. Mater.* **2021**, *7*, 612–620. [CrossRef]
6. Murmu, P.P.; Karthik, V.; Liu, Z.; Jovic, V.; Mori, T.; Yang, W.L.; Smith, K.E.; Kennedy, J.V. Influence of Carrier Density and Energy Barrier Scattering on a High Seebeck Coefficient and Power Factor in Transparent Thermoelectric Copper Iodide. *ACS Appl. Energy Mater.* **2020**, *3*, 10037–10044. [CrossRef]
7. Khedkar, R.S.; Shrivastava, N.; Sonawane, S.S.; Wasewar, K.L. Experimental investigations and theoretical determination of thermal conductivity and viscosity of TiO_2–ethylene glycol nanofluid. *Int. Commun. Heat Mass Transf.* **2016**, *73*, 54–61. [CrossRef]

8. Murshed, S.; Leong, K.; Yang, C. Thermophysical and electrokinetic properties of nanofluids—A critical review. *Appl. Therm. Eng.* **2008**, *28*, 2109–2125. [CrossRef]
9. Saidur, R.; Leong, K.Y.; Mohammed, H.A. A review on applications and challenges of nanofluids. *Renew. Sustain. Energy Rev.* **2011**, *15*, 1646–1668. [CrossRef]
10. Sidik, N.A.C.; Kean, T.H.; Chow, H.K.; Rajaandra, A.; Rahman, S.; Kaur, J. Performance enhancement of cold thermal energy storage system using nanofluid phase change materials: A review. *Int. Commun. Heat Mass Transf.* **2018**, *94*, 85–95. [CrossRef]
11. Muhammad, M.J.; Muhammad, I.A.; Sidik, N.A.C.; Yazid, M.N.A.W.M. Thermal performance enhancement of flat-plate and evacuated tube solar collectors using nanofluid: A review. *Int. Commun. Heat Mass Transf.* **2016**, *76*, 6–15. [CrossRef]
12. Soltani, S.; Kasaeian, A.; Sarrafha, H.; Wen, D. An experimental investigation of a hybrid photovoltaic/thermoelectric system with nanofluid application. *Sol. Energy* **2017**, *155*, 1033–1043. [CrossRef]
13. Senthilraja, S.; Karthikeyan, M.; Gangadevi, R. Nanofluid applications in future automobiles: Comprehensive review of existing data. *Nano-Micro Lett.* **2010**, *2*, 306–310. [CrossRef]
14. Sundar, L.S.; Singh, M.K.; Sousa, A.C. Investigation of thermal conductivity and viscosity of Fe_3O_4 nanofluid for heat transfer applications. *Int. Commun. Heat Mass Transf.* **2013**, *44*, 7–14. [CrossRef]
15. Hatami, M.; Mohammadi-Rezaei, S.; Tahari, M.; Jing, D. Recent developments in magneto-hydrodynamic Fe_3O_4 nanofluids for different molecular applications: A review study. *J. Mol. Liq.* **2018**, *250*, 244–258. [CrossRef]
16. Usri, N.A.; Azmi, W.H.; Mamat, R.; Hamid, K.A.; Najafi, G. Thermal conductivity enhancement of Al_2O_3 nanofluid in ethylene glycol and water mixture. *Energy Procedia* **2015**, *79*, 397–402. [CrossRef]
17. Hong, T.K.; Yang, H.S.; Choi, C. Study of the enhanced thermal conductivity of Fe nanofluids. *J. Appl. Phys.* **2005**, *97*, 064311. [CrossRef]
18. Batmunkh, M.; Tanshen, M.R.; Nine, M.J.; Myekhlai, M.; Choi, H.; Chung, H.; Jeong, H. Thermal conductivity of TiO_2 nanoparticles based aqueous nanofluids with an addition of a modified silver particle. *Ind. Eng. Chem. Res.* **2014**, *53*, 8445–8451. [CrossRef]
19. Berg, J.C. *An Introduction to Interfaces & Colloids: The Bridge to Nanoscience*; World Scientific: Singapore, 2010.
20. Otero-Lorenzo, R.; Ramos-Docampo, M.A.; Rodriguez-Gonzalez, B.; Comesaña-Hermo, M.; Salgueiriño, V. Solvothermal clustering of magnetic spinel ferrite nanocrystals: A Raman perspective. *Chem. Mater.* **2017**, *29*, 8729–8736. [CrossRef]
21. Otero-Lorenzo, R.; Fantechi, E.; Sangregorio, C.; Salgueiriño, V. Solvothermally driven Mn doping and clustering of iron oxide nanoparticles for heat delivery applications. *Chem. Eur. J.* **2016**, *22*, 6666–6675. [CrossRef]
22. Izadkhah, M.S.; Erfan-Niya, H.; Moradkhani, H. Rheological Behavior of Water-Ethylene Glycol Based Graphene Oxide Nanofluids. *Iran. J. Chem. Chem. Eng.* **2018**, *37*, 177–187.
23. Kumar, R.S.; Sharma, T. Stability and rheological properties of nanofluids stabilized by SiO_2 nanoparticles and SiO_2-TiO_2 nanocomposites for oilfield applications. *Colloid Surf. A Physicochem. Eng. Asp.* **2018**, *539*, 171–183. [CrossRef]
24. Elsaidy, A.; Vallejo, J.P.; Salgueiriño, V.; Lugo, L. Tuning the thermal properties of aqueous nanofluids by taking advantage of size-customized clusters of iron oxide nanoparticles. *J. Mol. Liq.* **2021**, *344*, 117727. [CrossRef]
25. Lu, Z.; Yin, Y. Colloidal nanoparticle clusters: Functional materials by design. *Chem. Soc. Rev.* **2012**, *41*, 6874–6887. [CrossRef]
26. Xuan, S.; Wang, F.; Wang, Y.X.J.; Jimmy, C.Y.; Leung, K.C.F. Facile synthesis of size-controllable monodispersed ferrite nanospheres. *J. Mater. Chem.* **2010**, *20*, 5086–5094. [CrossRef]
27. Deng, H.; Li, X.; Peng, Q.; Wang, X.; Chen, J.; Li, Y. Monodisperse magnetic single-crystal ferrite microspheres. *Angew. Chem.* **2005**, *117*, 2842–2845. [CrossRef]
28. Reddy, M.P.; Mohamed, A.M.A.; Zhou, X.B.; Du, S.; Huang, Q. A facile hydrothermal synthesis, characterization and magnetic properties of mesoporous $CoFe_2O_4$ nanospheres. *J. Magn. Magn. Mater.* **2015**, *388*, 40–44. [CrossRef]
29. *D7896-19*; Standard Test Method for Thermal Conductivity, Thermal Diffusivity, and Volumetric Heat Capacity of Engine Coolants and Related Fluids by Transient Hot Wire Liquid Thermal Conductivity Method. ASTM International: West Conshohocken, PA, USA, 2019.
30. Sobczak, J.; Vallejo, J.P.; Traciak, J.; Hamze, S.; Fal, J.; Estellé, P.; Lugo, L.; Żyła, G. Thermophysical profile of ethylene glycol based nanofluids containing two types of carbon black nanoparticles with different specific surface areas. *J. Mol. Liq.* **2021**, *326*, 115255. [CrossRef]
31. Prado, J.I.; Calviño, U.; Lugo, L. Experimental methodology to determine thermal conductivity of nanofluids by using a commercial transient hot-wire device. *Appl. Sci.* **2021**, *12*, 329. [CrossRef]
32. Ramos-Docampo, M.A.; Testa-Anta, M.; Rivas-Murias, B.; Salgueiriño, V. Clusters of Magnetite-Maghemite Nanocrystals with a Chemically-Tailored Average Diameter. *J. Nanosci. Nanotechnol.* **2019**, *19*, 4930–4937. [CrossRef]
33. Ferreira, T.A.S.; Waerenborgh, J.C.; Mendonça, M.H.R.M.; Nunes, M.R.; Costa, F.M. Structural and morphological characterization of $FeCo_2O_4$ and $CoFe_2O_4$ spinels prepared by a coprecipitation method. *Solid State Sci.* **2003**, *5*, 383–392. [CrossRef]
34. Scott, J. Soft-mode spectroscopy: Experimental studies of structural phase transitions. *Rev. Mod. Phys.* **1974**, *46*, 83. [CrossRef]
35. Rivas-Murias, B.; Testa-Anta, M.; Torruella, P.; Estradé, S.; Peiró, F.; Rodríguez-González, B.; Comesaña-Hermo, M.; Salgueiriño, V. Structural and magnetic implications of transition metal migration within octahedral core–Shell nanocrystals. *Chem. Mater.* **2020**, *32*, 10435–10446. [CrossRef]
36. Testa-Anta, M.; Rivas-Murias, B.; Salgueiriño, V. Spin frustration drives exchange bias sign crossover in $CoFe_2O_4$–Cr_2O_3 nanocomposites. *Adv. Funct. Mater.* **2019**, *29*, 1900030. [CrossRef]

37. Sanles-Sobrido, M.; Bañobre-López, M.; Salgueirino, V.; Correa-Duarte, M.A.; Rodríguez-González, B.; Rivas, J.; Liz-Marzán, L.M. Tailoring the magnetic properties of nickel nanoshells through controlled chemical growth. *J. Mater. Chem.* **2010**, *20*, 7360–7365. [CrossRef]
38. Sharma, S.; Gupta, S.M. Preparation and evaluation of stable nanofluids for heat transfer application: A review. *Exp. Therm. Fluid Sci.* **2016**, *79*, 202–212.
39. Vallejo, J.P.; Mercatelli, L.; Martina, M.R.; Di Rosa, D.; Dell'Oro, A.; Lugo, L.; Sani, E. Comparative study of different functionalized graphene-nanoplatelet aqueous nanofluids for solar energy applications. *Renew. Energy* **2019**, *141*, 791–801. [CrossRef]
40. Lemmon, E.W.; Bell, I.H.; Huber, M.L.; McLinden, M.O. *NIST Standard Reference Database 23: Reference Fluid Thermodynamic and Transport Properties-REFPROP, Version 10.0, National Institute of Standards and Technology*; Standard Reference Data Program: Gaithersburg, MD, USA, 2018.
41. Melinder, A. *Properties of Secondary Working Fluids for Indirect Systems*; International Institute of Refrigeration: Paris, France, 2010.
42. Sun, T.; Teja, A.S. Density, viscosity and thermal conductivity of aqueous solutions of propylene glycol, dipropylene glycol, and tripropylene glycol between 290 K and 460 K. *J. Chem. Eng. Data* **2004**, *49*, 1311–1317. [CrossRef]
43. Chon, C.H.; Kihm, K.D.; Lee, S.P.; Choi, S.U.S. Empirical correlation finding the role of temperature and particle size for nanofluid (Al2O3) thermal conductivity enhancement. *Appl. Phys. Lett.* **2005**, *87*, 153107. [CrossRef]
44. Li, C.H.; Peterson, G. The effect of particle size on the effective thermal conductivity of Al_2O_3-water nanofluids. *J. Appl. Phys.* **2007**, *101*, 044312. [CrossRef]
45. Mintsa, H.A.; Roy, G.; Nguyen, C.T.; Doucet, D. New temperature dependent thermal conductivity data for water-based nanofluids. *Int. J. Therm. Sci.* **2009**, *48*, 363–371. [CrossRef]
46. Lee, J.H.; Lee, S.H.; Pil Jang, S. Do temperature and nanoparticle size affect the thermal conductivity of alumina nanofluids? *Appl. Phys. Lett.* **2014**, *104*, 161908. [CrossRef]
47. Patel, H.E.; Sundararajan, T.; Das, S.K. An experimental investigation into the thermal conductivity enhancement in oxide and metallic nanofluids. *J. Nanopart. Res.* **2010**, *12*, 1015–1031. [CrossRef]
48. He, Y.; Jin, Y.; Chen, H.; Ding, Y.; Cang, D.; Lu, H. Heat transfer and flow behaviour of aqueous suspensions of TiO_2 nanoparticles (nanofluids) flowing upward through a vertical pipe. *Int. J. Heat Mass Transf.* **2007**, *50*, 2272–2281. [CrossRef]
49. Maheshwary, P.; Handa, C.; Nemade, K. A comprehensive study of effect of concentration, particle size and particle shape on thermal conductivity of titania/water based nanofluid. *Appl. Therm. Eng.* **2017**, *119*, 79–88. [CrossRef]
50. Kim, S.H.; Choi, S.R.; Kim, D. Thermal conductivity of metal-oxide nanofluids: Particle size dependence and effect of laser irradiation. *J. Heat Transf.* **2007**, *129*, 298–307. [CrossRef]
51. Timofeeva, E.V.; Routbort, J.L.; Singh, D. Particle shape effects on thermophysical properties of alumina nanofluids. *J. Appl. Phys.* **2009**, *106*, 014304. [CrossRef]
52. Vajjha, R.S.; Das, D.K. Experimental determination of thermal conductivity of three nanofluids and development of new correlations. *Int. J. Heat Mass Transf.* **2009**, *52*, 4675–4682. [CrossRef]
53. Chen, G.; Yu, W.; Singh, D.; Cookson, D.; Routbort, J. Application of SAXS to the study of particle-size-dependent thermal conductivity in silica nanofluids. *J. Nanopart. Res.* **2008**, *10*, 1109–1114. [CrossRef]
54. Sun, C.; Bai, B.; Lu, W.Q.; Liu, J. Shear-rate dependent effective thermal conductivity of H_2O+SiO_2 nanofluids. *Phys. Fluids* **2013**, *25*, 052002. [CrossRef]
55. Murshed, S.; Leong, K.; Yang, C. Enhanced thermal conductivity of TiO_2—Water based nanofluids. *Int. J. Therm. Sci.* **2005**, *44*, 367–373. [CrossRef]
56. Pryazhnikov, M.I.; Minakov, A.V.; Rudyak, V.Y.; Guzei, D.V. Thermal conductivity measurements of nanofluids. *Int. J. Heat Mass Transf.* **2017**, *104*, 1275–1282. [CrossRef]
57. Satti, J.R.; Das, D.K.; Ray, D. Investigation of the thermal conductivity of propylene glycol nanofluids and comparison with correlations. *Int. J. Heat Mass Transf.* **2017**, *107*, 871–881. [CrossRef]
58. Ambreen, T.; Kim, M.H. Influence of particle size on the effective thermal conductivity of nanofluids: A critical review. *Appl. Energy* **2020**, *264*, 114684. [CrossRef]
59. Beck, M.P.; Yuan, Y.; Warrier, P.; Teja, A.S. The thermal conductivity of alumina nanofluids in water, ethylene glycol, and ethylene glycol+ water mixtures. *J. Nanopart. Res.* **2010**, *12*, 1469–1477. [CrossRef]
60. Agromayor, R.; Cabaleiro, D.; Pardiñas, A.A.; Vallejo, J.P.; Fernandez-Seara, J.; Lugo, L. Heat transfer performance of functionalized graphene nanoplatelet aqueous nanofluids. *Materials* **2016**, *9*, 455. [CrossRef]
61. Vallejo, J.P.; Pérez-Tavernier, J.; Cabaleiro, D.; Fernández-Seara, J.; Lugo, L. Potential heat transfer enhancement of functionalized graphene nanoplatelet dispersions in a propylene glycol-water mixture. Thermophysical profile. *J. Chem. Thermodyn.* **2018**, *123*, 174–184. [CrossRef]
62. Yu, W.; Xie, H.; Chen, L.; Li, Y. Enhancement of thermal conductivity of kerosene-based Fe_3O_4 nanofluids prepared via phase-transfer method. *Colloids Surf. A Physicochem. Eng. Asp.* **2010**, *355*, 109–113. [CrossRef]
63. Hadadian, M.; Goharshadi, E.K.; Youssefi, A. Electrical conductivity, thermal conductivity, and rheological properties of graphene oxide-based nanofluids. *J. Nanopart. Res.* **2014**, *16*, 2788. [CrossRef]
64. Fu, R.; Liu, Z.; Chen, Y.; Yan, Y. Experimental investigation of turbulent forced heat transfer of Fe_3O_4 ethylene glycol–water nanofluid with highly disaggregated particles. *Therm. Sci. Eng. Prog.* **2019**, *10*, 1–9. [CrossRef]

65. Esfe, M.H.; Afrand, M.; Karimipour, A.; Yan, W.M.; Sina, N. An experimental study on thermal conductivity of MgO nanoparticles suspended in a binary mixture of water and ethylene glycol. *Int. Commun. Heat Mass Transf.* **2015**, *67*, 173–175. [CrossRef]
66. Abdolbaqi, M.K.; Azmi, W.H.; Mamat, R.; Sharma, K.V.; Najafi, G. Experimental investigation of thermal conductivity and electrical conductivity of BioGlycol–water mixture based Al_2O_3 nanofluid. *Appl. Therm. Eng.* **2016**, *102*, 932–941. [CrossRef]
67. Kharat, P.B.; Kounsalye, J.S.; Shisode, M.V.; Jadhav, K.M. Preparation and thermophysical investigations of $CoFe_2O_4$-based nanofluid: A potential heat transfer agent. *J. Supercond. Nov. Magn.* **2019**, *32*, 341–351. [CrossRef]
68. Vallejo, J.P.; Gomez-Barreiro, S.; Cabaleiro, D.; Gracia-Fernandez, C.; Fernandez-Seara, J.; Lugo, L. Flow behaviour of suspensions of functionalized graphene nanoplatelets in propylene glycol–water mixtures. *Int. Commun. Heat Mass Transf.* **2018**, *91*, 150–157. [CrossRef]
69. Das, P.K. A review based on the effect and mechanism of thermal conductivity of normal nanofluids and hybrid nanofluids. *J. Mol. Liq.* **2017**, *240*, 420–446. [CrossRef]

Disclaimer/Publisher's Note: The statements, opinions and data contained in all publications are solely those of the individual author(s) and contributor(s) and not of MDPI and/or the editor(s). MDPI and/or the editor(s) disclaim responsibility for any injury to people or property resulting from any ideas, methods, instructions or products referred to in the content.